

Step-aware Preference Optimization: Aligning Preference with Denoising Performance at Each Step

Zhanhao Liang[†] Yuhui Yuan Shuyang Gu Bohan Chen[†] Tiankai Hang[†] Ji Li Liang Zheng
 {yuyua, shuyangu}@microsoft.com, liang.zheng@anu.edu.au
 The Australian National University University of Liverpool Southeast University
 Microsoft Research Asia

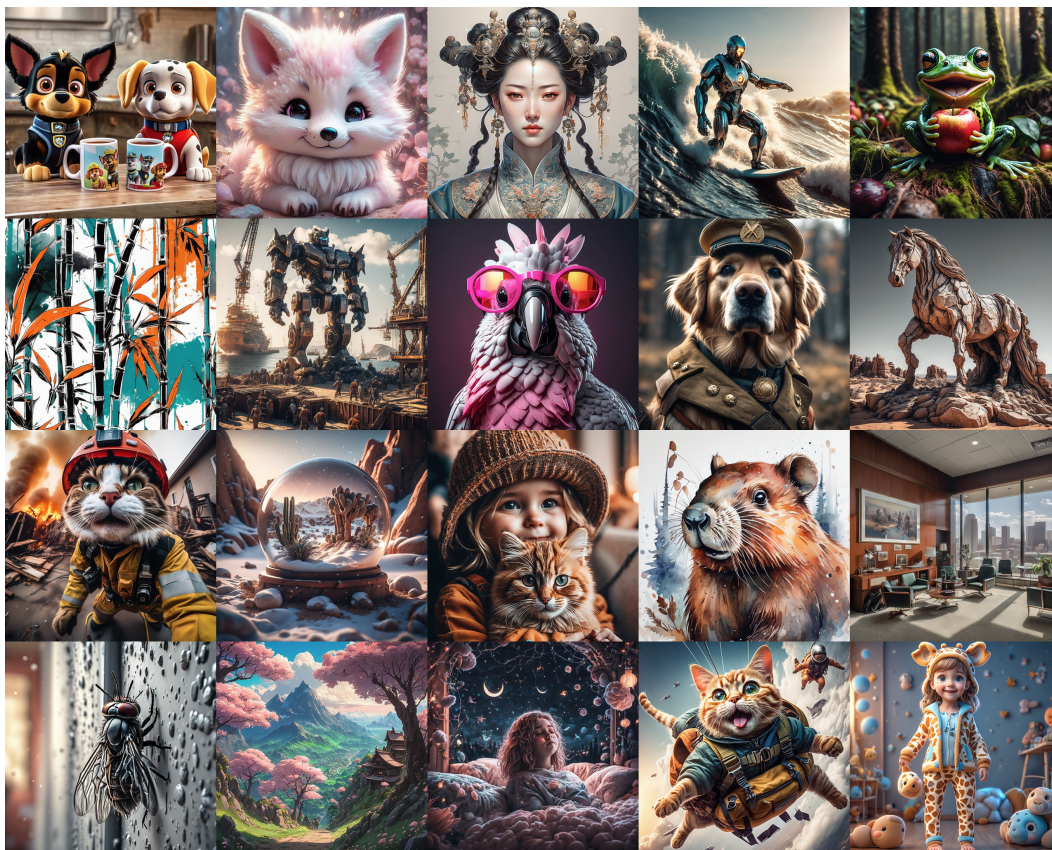


Figure 1: Sample images generated by SDXL fine-tuned using our step-aware preference optimization (SPO). SPO aligns the step-wise human preference at the corresponding denoising step. With the SPO post-training, SDXL produces high-quality images that not only better follow the text prompt but also more visually attractive and stunning.

Abstract

Recently, Direct Preference Optimization (DPO) has extended its success from aligning large language models (LLMs) to aligning text-to-image diffusion models with human preferences. Unlike most existing DPO methods that assume all diffusion steps share a consistent preference order with the final generated images, we argue that this assumption neglects step-specific denoising performance and that

[†]Interns at Microsoft Research Asia.

preference labels should be tailored to each step’s contribution. To address this limitation, we propose Step-aware Preference Optimization (SPO), a novel post-training approach that independently evaluates and adjusts the denoising performance at each step, using a *step-aware preference model* and a *step-wise resampler* to ensure accurate step-aware supervision. Specifically, at each denoising step, we sample a pool of images, find a suitable win-lose pair, and, most importantly, randomly select a single image from the pool to initialize the next denoising step. This step-wise resampler process ensures the next win-lose image pair comes from the same image, making the win-lose comparison independent of the previous step. To assess the preferences at each step, we train a separate step-aware preference model that can be applied to both noisy and clean images. Our experiments with Stable Diffusion v1.5 and SDXL demonstrate that SPO significantly outperforms the latest Diffusion-DPO in aligning generated images with complex, detailed prompts and enhancing aesthetics, while also achieving more than $20\times$ times faster in training efficiency. Code and model: <https://rockeycoss.github.io/spo.github.io/>

1 Introduction

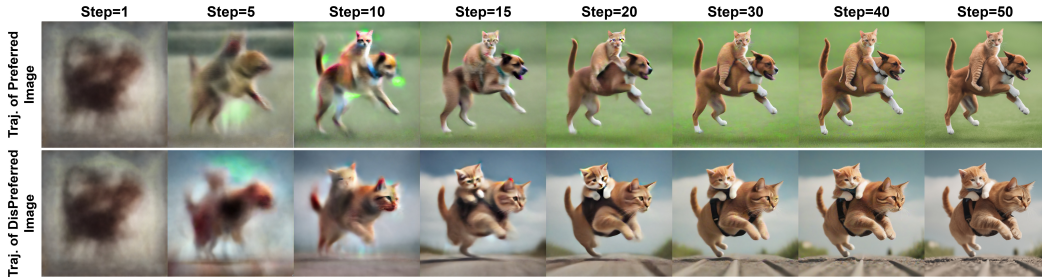


Figure 2: Two denoising trajectories of a preferred image and a dispreferred image generated from the same prompt “A **cat** jumps on a **dog**.” The final image of the upper trajectory is preferred for correctly generating a dog and a cat in a correct spatial arrangement. However, in terms of the quality of high-frequency details and naturalness, the final image of the lower trajectory is better. Therefore, the preference label applied in the later steps might provide incorrect signals.

This paper studies the use of direct preference optimization (DPO) Rafailov et al. [2024], Yang et al. [2023], Wallace et al. [2023] for the post-training of text-to-image diffusion models. When presented with a pair of images generated from the same prompt, where one is preferred and the other is dispreferred, DPO-based methods improve the diffusion model by encouraging its predictions to more closely align with the preferred image while concurrently discouraging them from resembling the dispreferred image.

This paper makes two observations regarding DPO optimization. First, we note that a diffusion model is a multi-step generation process, wherein the DPO’s loss function imparts supervision at the trajectory level. Consequently, most existing approaches Wallace et al. [2023], Yang et al. [2023] apply it uniformly across all intermediate generation steps. However, we point out that the supervision signal—specifically, the win-lose preference label—should reflect the denoising performance at each step, respectively.

On the other hand, it has been reported Hertz et al. [2022] that different diffusion steps have different generation focuses. For example, early steps tend to generate layout, while later steps focus more on generating detailed textures. If a generated image has a dispreferred layout but good texture, it is expected that early denoising steps receive a ‘lose’ preference signal to improve its layout generation ability, while later steps receive a tie or even win signal. In other words, depending on the training images, denoising performance at different steps might be different, and thus their preference signals should also be different.

However, existing DPO methods for diffusion models assign the same preference of the output image to all the intermediate steps Yang et al. [2023], Wallace et al. [2023]. Fig. 2 illustrates how this would compromise DPO fine-tuning. The final image of the upper denoising trajectory is more preferred

than that of the lower trajectory because it has the correct layout and composition. However, the lower denoising trajectory constructs finer background details and more natural contact between the two animals in the later steps. For trajectory-level DPO methods Wallace et al. [2023], Yang et al. [2023], it is problematic to use the final preference for later steps because the label, which mainly comes from layout and composition preference, does not align with the comparison of image details, which is the focus of the later steps. This mismatch between label and function would compromise the fine-tuning of the denoising model.

To align the preference label and denoising performance at each step, we introduce step-aware preference optimization (SPO). Through SPO, we aim for (i) the denoising performance at each step to be assessed independently from previous steps and (ii) a step-aware win/lose/tie label to be given based on this independent assessment. To achieve this, we construct a step-aware preference model and design a step-wise resampling process for each denoising step. Specifically, starting from the noisy image x_t , we first denoise it multiple times to achieve a set of candidate images $\{x_s^1, x_s^2, \dots, x_s^k\}$, where $s < t$ and k is the number of candidate images. The step-aware preference model then assesses their quality and assigns a win/lose/tie label to the two images with the largest quality gap. Importantly, we randomly select a single image from those candidate images to initialize the denoising step s . In this manner, each denoising step is initialized from a single image. This means the image pair selected afterwards stems from the same noisy image, and thus their quality assessment reflects the denoising performance of this step alone.

With the above step-wise preference optimization mechanism, the preference of the current denoising step is independent from previous steps. To assess the accurate preference order for these intermediate steps, we further propose a step-aware preference model. To build a reliable step-aware preference model, we collect training data by adding various levels of noise to pairs of clean images and assume they have the same preference label as the clean images. We find that the preference model trained on this data has robust performance on intermediate steps with various noise levels.

Using the proposed SPO method, we fine-tune Stable Diffusion v1.5 (SD-1.5) Rombach et al. [2022] and SDXL Podell et al. [2023] to improve image-text alignment and the aesthetics of the generated images. We show that models fine-tuned by SPO yield more significant improvements over models fine-tuned by existing DPO methods under various evaluation metrics. Moreover, since the step-aware evaluator provides preference independently for each step, leading to more accurate preference labels, the training of our algorithm is $20\times$ times faster than the latest Diffusion-DPO Wallace et al. [2023]. We summarize the key contributions of this paper as follows:

- We point out that existing DPO methods for diffusion model fine-tuning intrinsically suffer from the mismatch between the step-aware denoising performance and the consistent preference label assumption based on the final generated images.
- We introduce a SPO (step-aware preference optimization) scheme to solve this problem. Through the combination of a step-aware preference model and a step-wise resampler scheme, SPO ensures that denoising performance is directly and independently assessed and thus better supervised.
- Our method significantly enhances the fine-tuning performance on SD-1.5 and SDXL and achieves $10\times$ times faster convergence compared the latest Diffusion-DPO Wallace et al. [2023].

2 Related Work

Recently, inspired by the success of post-training method, *e.g.*, reinforcement learning from human feedback (RLHF) Ouyang et al. [2022], on improving LLMs, various post-training methods are proposed to fine-tune pre-trained diffusion models to align human preferences. For example, Chen *et al.* Chen et al. [2023] leverage PPO Schulman et al. [2017] loss to fine-tune the text encoder of diffusion models. AligningT2I Lee et al. [2023] develops a reward model to evaluate the quality of generated images and subsequently fine-tunes the diffusion model using image-text pairs, weighted by assessment of the reward model. DPOK Fan et al. [2024] and DDPO Black et al. [2023] use policy gradient to fine-tune diffusion models, aiming at maximizing reward signals. Furthermore, ReFL Xu et al. [2024], DRaFT Clark et al. [2023], and AlignProp Prabhudesai et al. [2023] directly propagate the gradients through differentiable reward models to fine-tune the denoising steps. Inspired by the success of direct preference optimization (DPO) Rafailov et al. [2024], which has achieved success in the post-training of LLMs by eliminating the need for explicit reward models, the recent Diffusion-DPO Wallace et al. [2023] proposes to fine-tune diffusion models on the Pick-a-Pic Kirstain et al.

[2024] dataset that contains image preference pairs to improve the performance of diffusion models. In addition, D3PO Yang et al. [2023] proposes generating pairs of images from the same prompt and using a preference model or human evaluators to identify the preferred and dispreferred images. The very recent DenseReward method Yang et al. [2024] further proposes improving the DPO scheme with a temporal discounting approach that emphasizes the initial denoising steps. Despite such promising results, they suffer from misalignment between the preference for final images and the performance at each individual denoising step.

3 Direct Preference Optimization (DPO) Revisit

General formulation. Suppose we have a generation model π_θ , and when the input is i , the probability of generating o is $\pi_\theta(o | i)$. We use π_θ to generate the set of output pairs \mathcal{S} , where the outputs in each pair are generated from the same input i . Human or preference model is employed to label the preference order of outputs in the pairs as (o^w, o^l, i) , where o^w is the preferred output and o^l is the dispreferred output. According to Rafailov et al. [2024], the DPO loss $\mathcal{L}_{\mathcal{DPO}}$ used the fine-tune π_θ is defined as:

$$\mathcal{L}_{\mathcal{DPO}} = -\mathbb{E}_{(o^w, o^l, i) \sim \mathcal{S}} \left[\log \sigma \left(\beta \log \frac{\pi_\theta(o^w | i)}{\pi_{\text{ref}}(o^w | i)} - \beta \log \frac{\pi_\theta(o^l | i)}{\pi_{\text{ref}}(o^l | i)} \right) \right], \quad (1)$$

where π_{ref} refers to the reference model, which is usually the pre-trained model. σ refers to sigmoid function. β is a scalar controlling the strength of regularization.

Misaligned preference label and denoising performance at each step. In the context of text-to-image diffusion models, we denote the model parameter as p_θ , text prompt as c , the denoising process generates a sequence of intermediate states $\{\mathbf{x}_T, \mathbf{x}_{T-1}, \dots, \mathbf{x}_1, \mathbf{x}_0\}$. Existing works including Diffusion-DPO Wallace et al. [2023] and D3PO Yang et al. [2023] measures the quality according to the final generated image \mathbf{x}_0 , and assign the preference for \mathbf{x}_0 directly to the whole generation trajectory, in other words, all the intermediate states. We denote the denoising trajectories which generate the preferred and dispreferred image as \mathcal{T}_w and \mathcal{T}_l , respectively. Furthermore, leveraging the Markov property of diffusion models and the Jensen’s inequality, they split the general DPO loss in Eq. 1 into the following step-wise form:

$$\mathcal{L}_{\mathcal{DPO}-\mathcal{D}} = -\mathbb{E}_{(\mathbf{x}_{t-1}^w, \mathbf{x}_t^w) \sim \mathcal{T}_w, (\mathbf{x}_{t-1}^l, \mathbf{x}_t^l) \sim \mathcal{T}_l} \left[\log \sigma \left(\beta \log \frac{p_\theta(\mathbf{x}_{t-1}^w | \mathbf{x}_t^w, c)}{p_{\text{ref}}(\mathbf{x}_{t-1}^w | \mathbf{x}_t^w, c)} - \beta \log \frac{p_\theta(\mathbf{x}_{t-1}^l | \mathbf{x}_t^l, c)}{\pi_{\text{ref}}(\mathbf{x}_{t-1}^l | \mathbf{x}_t^l, c)} \right) \right], \quad (2)$$

where $\mathcal{L}_{\mathcal{DPO}-\mathcal{D}}$ encourages each timestep of denoising to progress more towards the preferred image and away from the dispreferred image.

We draw the training framework of Diffusion-DPO and D3PO in Fig. 3 (a) and (b), respectively. Although they differ in how to sampling from \mathcal{T}_w and \mathcal{T}_l , we can clearly see that both of them directly propagate preference label from \mathbf{x}_0 to intermediate states. That is, for \mathbf{x}_0^w , its predecessors along the win trajectory all share the same “preferred” label, and the same goes for the dispreferred trajectory. As mentioned in the introduction, this way of giving step-wise preference would deviate from the true preference for each denoising step: we would like to use the latter for supervision in our system.

4 Proposed Approach

To fundamentally address the misalignment between the preference for the final images and the performance at each individual denoising step, we propose a simple yet effective step-aware preference optimization scheme that explicitly evaluates the preference at each timestep and adjusts the step-wise denoising performance accordingly. First, we introduce the overall framework of our approach in Section 4.1. Second, we illustrate the details of three key technical contributions, including step-aware preference model in Section 4.2, step-wise resampler in Section 4.3, and our step-aware objective function in Section 4.4. Last, in Section 4.5, we emphasize that it is useful to extend to a multi-step-aware manner, which encourages the model to generate diverse results and achieve a better optimization direction.

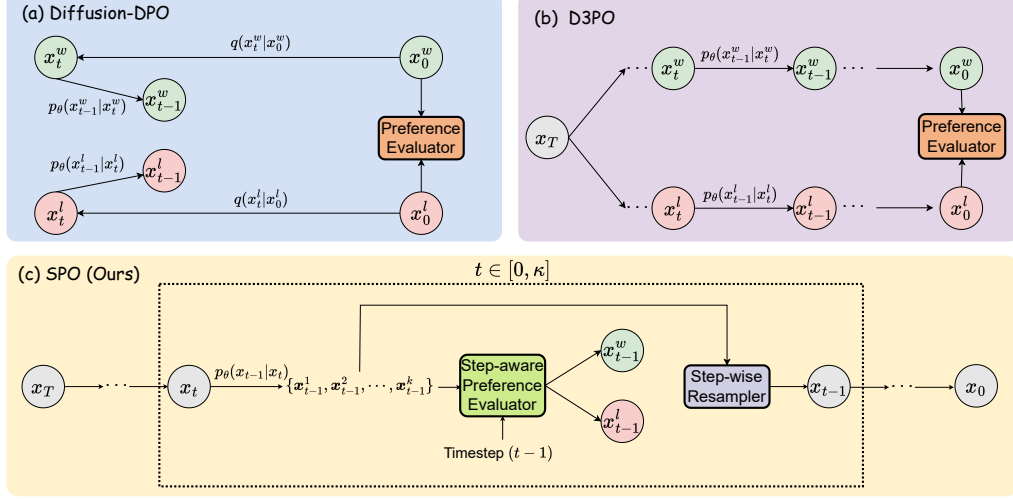


Figure 3: Comparing frameworks of SPO and the existing Diffusion-DPO and D3PO approaches. We apply the proposed step-aware preference evaluator and the step-wise resampler at each timestep.

4.1 Framework Overview

In order to accurately generate preference labels that can adaptively reflect how well each denoising timestep performs given the current noisy sample, we propose an online reinforcement learning method, *i.e.*, step-aware preference optimization, which follows a sample-then-update cycle during the training process. Specifically, given any time-step t , we first sample x_t starting from a Gaussian noise and sample a set of denoised samples at $(t-1)$ -th timestep $\{x_{t-1}^1, x_{t-1}^2, \dots, x_{t-1}^k\}$. Then we apply a step-aware preference model to compare all these candidate images, select the best-quality sample and the worst-quality sample as the win-sample and lose-sample, respectively, and estimate a preference direction for each denoising timestep accordingly. In addition, we highlight a step-wise resampling approach, which randomly selects a generated sample from the candidate set $\{x_{t-1}^1, x_{t-1}^2, \dots, x_{t-1}^k\}$ to ensure the independence of previous steps and augment the trajectory space. We illustrate the framework of SPO in Fig. 3 (c).

4.2 Step-aware Preference Model: Align the Preference with the Denoising Performance

To align the preference order at each timestep with the step-wise denoising performance, we first build a step-aware preference model. Unlike existing preference models that only can be applied to the final denoised images, our step-aware preference model takes the timestep t as a condition and predict preference on noisy intermediate images. We build the step-aware preference model by the drawing inspiration from the training process of noisy classifier Dhariwal and Nichol [2021], which is able to classify noisy intermediate images. We assume *the preference order between pair of images can be kept when adding the same noise*. Therefore, during training, given a pair of images and their corresponding preference labels, *e.g.*, x_0^w and x_0^l , we randomly sample a timestep t and employ diffusion process to add the same noise to both images to get x_t^w and x_t^l . Then we feed the noisy image pair $\{x_t^w, x_t^l\}$ and the timestep t to the step-aware preference model and train the model to correctly predict the preference, following $\mathcal{L}_{\text{pref}} = (\log 1 - \log \hat{p}_w)$ as in Kirstain et al. [2024]. We also compute the loss for the tie pairs, and we show how to estimate \hat{p}_w as follows:

$$\hat{p}_w = \frac{\exp(\tau \cdot f_{\text{CLIP-V}}(x_t^w, t) \cdot f_{\text{CLIP-T}}(c))}{\exp(\tau \cdot f_{\text{CLIP-V}}(x_t^w, t) \cdot f_{\text{CLIP-T}}(c)) + \exp(\tau \cdot f_{\text{CLIP-V}}(x_t^l, t) \cdot f_{\text{CLIP-T}}(c))}, \quad (3)$$

where c represents the text prompt and we modify the CLIP vision encoder within the preference model following the time-conditional adaptive layernorm Peebles and Xie [2023] to support timestep-conditional preference prediction. After training, the step-aware preference model can be used to predict the preference order among k sampled denoised samples $\{x_{t-1}^1, x_{t-1}^2, \dots, x_{t-1}^k\}$.

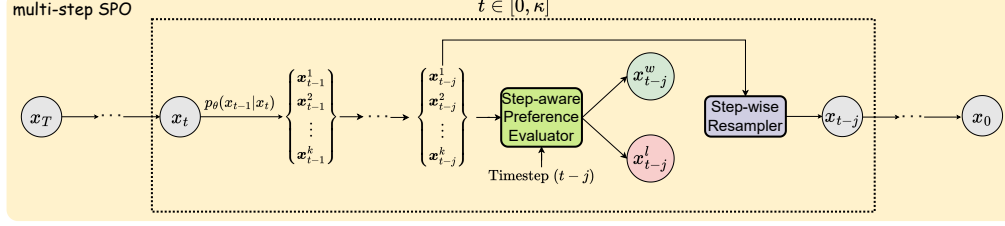


Figure 4: Framework of multi-step-aware SPO. We first sample k independent multi-step (e.g., j timesteps) denoising trajectories to obtain $\{x_{t-1}^1, x_{t-1}^2, \dots, x_{t-1}^k\}$. Then we apply the step-aware preference model and the step-wise resampler in the same manner as SPO.

4.3 Step-wise Resampler: Remove the Trajectory-level Dependency

The key insight of step-wise resampling is in redesigning the choice of x_t at the t -th denoise timestep to avoid the preference propagation from the previous denoising steps. First, we illustrate how Diffusion-DPO and D3PO determine x_t^w and x_t^l as follows: (i) Diffusion-DPO samples x_t^w or x_t^l by directly adding t timesteps of noise to the win image x_0^w or lose image x_0^l , i.e., $x_t \sim q(x_t | x_0)$, $x_0 \in \mathcal{I}$, where \mathcal{I} is the set of all win-lose pairs; (ii) D3PO first samples two independent entire trajectories like $\mathcal{T}_w = \{x_T, x_{T-1}^w, \dots, x_0^w\}$ and $\mathcal{T}_l = \{x_T, x_{T-1}^l, \dots, x_0^l\}$ and then samples the corresponding samples at the t -th timestep, i.e., x_t^w and x_t^l . We illustrate their approach in Fig. 3. Contrary to them, our approach randomly samples one x_t , by denoising from random Gaussian noise, instead of selecting a pair of win-lose samples. The idea of *sampling the follow-up denoised samples x_{t-1}^w and x_{t-1}^l starting from a single shared latent x_t is the key to removing the dependency on the previous denoising performance or the preference order over the final output.*

It is obvious that we share the same noise latent x_T with $t = T$. When $t < T$, we also random sample x_t from a small set of k candidates, e.g., $\{x_t^1, x_t^2, \dots, x_t^k\}$, denoised from the previous noisy latent x_{t+1} following $x_t \sim p_\theta(x_t | x_{t+1}, c)$. We propose three different resampling strategies, including: (i) always selecting the win sample from the candidate set; (ii) always selecting the lose sample from the candidate set; (iii) randomly selecting a sample from the candidate set. After determining the choice of x_t , we send it into the next denoising timestep. We illustrate the position of the step-wise resampler within our entire framework in Fig. 3 (c), where we take the selection of x_{t-1} as an example for consistency with the above discussion. We empirically find that the step-aware resampler based on random selection achieves the best performance.

4.4 Step-aware Objective Function

At the t -th denoising timestep, we sample a small set $\{x_{t-1}^1, x_{t-1}^2, \dots, x_{t-1}^k\}$ and use the step-aware preference model to construct a preference pair (x_{t-1}^w, x_{t-1}^l) , where x_{t-1}^w is the most preferred and x_{t-1}^l is most dispreferred among the candidate set. By sampling from various prompts, we can obtain a set of preference pairs at t -th timestep. Referring to the general form of DPO loss in Eq.1, the DPO objective at t -th timestep is as follows:

$$\mathcal{L}_t(\theta) = -\mathbb{E}_{c \sim p(c), x_{t-1}^w, x_{t-1}^l \sim p_\theta(x_{t-1} | c, t, x_t)} \left[\log \sigma \left(\beta \log \frac{p_\theta(x_{t-1}^w | c, t, x_t)}{p_{\text{ref}}(x_{t-1}^w | c, t, x_t)} - \beta \log \frac{p_\theta(x_{t-1}^l | c, t, x_t)}{p_{\text{ref}}(x_{t-1}^l | c, t, x_t)} \right) \right], \quad (4)$$

where c refers to the prompt and $p(c)$ is the distribution of prompts.

Then by combining the DPO objectives across all T timesteps, we can get the final DPO objective for step-aware preference optimization training:

$$\mathcal{L}(\theta) = -\mathbb{E}_{t \sim \mathcal{U}[1, T], c \sim p(c), x_T \sim \mathcal{N}(\mathbf{0}, \mathbf{I}), x_{t-1}^w, x_{t-1}^l \sim p_\theta(x_{t-1} | c, t, x_t)} \left[\log \sigma \left(\beta \log \frac{p_\theta(x_{t-1}^w | c, t, x_t)}{p_{\text{ref}}(x_{t-1}^w | c, t, x_t)} - \beta \log \frac{p_\theta(x_{t-1}^l | c, t, x_t)}{p_{\text{ref}}(x_{t-1}^l | c, t, x_t)} \right) \right], \quad (5)$$

where \mathcal{U} refers to uniform distribution and \mathcal{N} refers to gaussian distribution.

Method	PickScore	HPSV2	ImageReward	Aesthetic
SDXL	21.95	26.95	0.5380	5.950
Diff.-DPO	22.64	29.31	0.9436	6.015
SPO	<u>23.06</u>	<u>31.80</u>	<u>1.0803</u>	<u>6.364</u>

Table 1: Comparison of AI feedback on SDXL. SPO overall yields the best fine-tuning performance.

Method	PickScore	HPSV2	ImageReward	Aesthetic
SD-1.5	20.53	23.79	-0.1628	5.365
DDPO	21.06	24.91	0.0817	5.591
D3PO	20.76	23.97	-0.1235	5.527
Diff.-DPO	20.98	25.05	0.1115	5.505
SPO	<u>21.43</u>	<u>26.45</u>	<u>0.1712</u>	<u>5.887</u>

Table 2: Comparing AI feedback on SD-1.5.

4.5 Extension to Multi-step-aware Preference Optimization

We empirically observe that due to the minimal differences between x_t and x_{t-1} , the selected candidates \mathbf{x}_{t-1}^w and \mathbf{x}_{t-1}^l also exhibit very small disparities. Consequently, we expand step-aware preference optimization to multi-step-aware preference optimization, employing multiple denoising processes to increase the diversity of the candidate set, as shown in Figure 4. This simple extension allows us to select superior samples, and make training more efficient. We find this approach very useful in finetuning stronger diffusion models like SDXL. In section 5.3, we conduct experiments to verify its effectiveness and further explore the impact of various implementation methods on fine-tuning performance.

5 Experiments

5.1 Experimental Setup

We follow the best official settings of Diffusion-DPO, DDPO, and D3PO to ensure fair comparisons. Diffusion-DPO requires fine-tuning SDXL on the entire Pick-a-Pic V2 dataset, which consists of over 850K win-lose image pairs. All other methods, including ours, are fine-tuned on a set of 4K prompts randomly selected from Pick-a-Pic V1 and generate win-lose pairs online.

We apply DDIM Song et al. [2020] with $\eta = 1.0$ and 20 timesteps as the sampler and use classifier free guidance Ho and Salimans [2022] with scale 5.0 during sampling. We utilize the LoRA Hu et al. [2021] technique for both SD-1.5 and SDXL, fine-tuning the models for ~ 10 epochs. The LoRA rank is 4 and 64 for SD-1.5 and SDXL, respectively. We set the strength of regularization $\beta = 10$. For SD-1.5, we set the batch size as 40 and the learning rate as $6e^{-5}$. For SDXL, we set the batch size as 8, the gradient accumulation as 2, and the learning rate as $1e^{-5}$. Since the step-aware preference model has difficulty determining preference orders at large timestep range, we only order the preference of x_t with $t \leq \kappa$ and consider x_t with $t > \kappa$ as tied. We empirically find setting κ as 750 achieves the best performance. When fine-tuning SDXL, to increase the differences between x_{t-1} , we set the number of inner steps to ~ 3 . Notably, we do not apply the SDXL refiner in any of our experiments by default to ensure fair comparisons.

We implement the step-aware preference model by modifying the PickScore Kirstain et al. [2024] model² into our step-aware preference model as follows. First, we inject the time condition into the vision encoder of PickScore by applying adaptive layer normalization after each attention layer and FFN layer, following the adaptive layer norm (adaLN) block design of DiT Peebles and Xie [2023]. Then, we fine-tune the modified model on the human preference pairs dataset, Pick-a-Pic Kirstain et al. [2024]. We randomly sample a timestep t from the range $[0, 1000]$ and apply the diffusion process to add t steps of noise to a pair of win-lose images during fine-tuning. To alleviate the domain gap between the noised image at the t -th timestep and the original images used to train the PickScore model, we choose to estimate \hat{x}_0 from the noisy sample directly, following the DDIM Song et al. [2020] scheme. Finally, we send the estimated pairs of win-lose images and their corresponding prompts into the modified step-aware preference model, *i.e.*, step-aware PickScore, and further fine-tune the step-aware preference model to learn to predict the preference order conditioned on the noised samples at different noise steps.

²PickScore is a refined CLIP Radford et al. [2021] model that can predict human preferences given pairs of images generated from the same prompt.

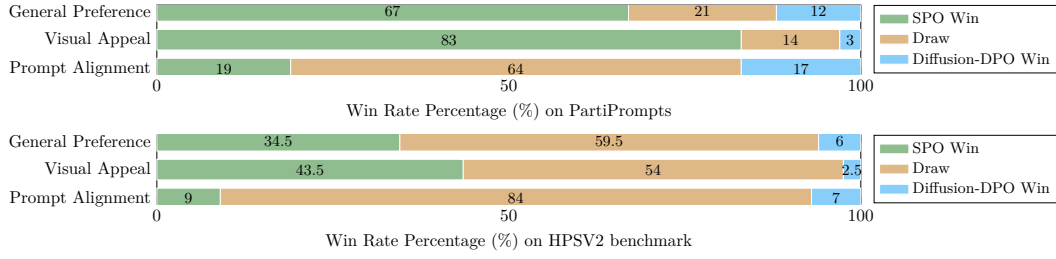


Figure 5: User study results comparing SPO and Diffusion-DPO based on SDXL. We follow Wallace et al. [2023] to generate images on both Partiprompts Yu et al. [2022] and HPS Wu et al. [2023b]. SPO achieves better performance in both aspects, including “general preference” and “visual appeal.”



Figure 6: Qualitative comparison between Diffusion-DPO and SPO based on SDXL. The prompts from top left to bottom right are: (1) Saturn rises on the horizon. (2) A kitchen. (3) A galaxy-colored figurine floating over the sea at sunset, photorealistic. (4) In a fantastical setting, a highly detailed furry humanoid skunk with piercing eyes confidently poses in a medium shot, wearing an animal hide jacket. The artist has masterfully rendered the character in digital art, capturing the intricate details of fur and clothing texture. (5) A swirling, multicolored portal emerges from the depths of an ocean of coffee, with waves of the rich liquid gently rippling outward. The portal engulfs a coffee cup, which serves as a gateway to a fantastical dimension. The surrounding digital art landscape reflects the colors of the portal, creating an alluring scene of endless possibilities. (6) A profile picture of an anime boy, half robot, brown hair (7) An astronaut riding a pig, highly realistic dslr photo, cinematic shot. (8) On the Mid-Autumn Festival, the bright full moon hangs in the night sky. A quaint pavilion is illuminated by dim lights, resembling a beautiful scenery in a painting. Camera type: close-up. Camera lens type: telephoto. Time of day: night. Style of lighting: bright. Film type: ancient style. HD.

Resampler	PickScore	HPSV2	ImageReward	Aesthetics
\mathbf{x}	20.63	24.37	-0.0260	5.438
\mathbf{x}_{t-1}^w	17.87	11.31	-2.2692	3.963
\mathbf{x}_{t-1}^l	19.36	18.63	-1.3743	5.338
random	<u>21.43</u>	<u>26.45</u>	<u>0.1712</u>	<u>5.887</u>

Table 3: Comparing different strategies in step-wise resampler. ‘Random’ has the best performance. This demonstrates the importance of step-aware resampling.

# samples k	PickScore	HPSV2	ImageReward	Aesthetics
2	21.37	26.56	0.3235	5.714
4	<u>21.43</u>	<u>26.45</u>	<u>0.1712</u>	<u>5.887</u>
8	21.19	<u>27.62</u>	<u>0.4199</u>	5.605

Table 5: Impact of number of sampled images at each denoising step. We use four images in the paper.

κ	PickScore	HPSV2	ImageReward	Aesthetics
250	20.61	23.34	-0.1823	5.413
500	20.69	25.67	0.0810	5.399
750	<u>21.43</u>	<u>26.45</u>	<u>0.1712</u>	<u>5.887</u>
1000	19.77	22.72	-0.4529	5.111

Table 7: Effect of the timestep range κ .

Preference model	PickScore	HPSV2	ImageReward	Aesthetics
PickScore	20.28	23.09	-0.2982	5.410
PickScore + step-agnostic	21.19	25.84	0.1365	5.678
PickScore + step-aware	<u>21.43</u>	<u>26.45</u>	<u>0.1712</u>	<u>5.887</u>

Table 4: Comparing the step-aware preference model with its step-agnostic version which removes the timestep condition. Being ‘step-aware’ is superior.

# inner steps j	PickScore	HPSV2	ImageReward	Aesthetics
1	22.85	31.37	1.0071	6.359
2	22.84	31.17	1.0118	6.268
3	22.94	31.55	<u>1.0847</u>	6.380
4	<u>23.06</u>	<u>31.80</u>	1.0803	6.364
5	23.03	31.23	0.9656	<u>6.423</u>
6	22.95	30.57	0.9770	6.390

Table 6: Effect of # inner steps when fine-tuning SDXL with SPO. We choose to use three four steps.

win-lose sample	PickScore	HPSV2	ImageReward	Aesthetics
best + worst	<u>21.43</u>	<u>26.45</u>	<u>0.1712</u>	<u>5.887</u>
random	21.21	<u>26.51</u>	0.1656	5.796

Table 8: Effect of the win-lose pairs choice.

5.2 Comparison with the State-of-the-art Methods

To verify the effectiveness of our approach, we compare our approach with the state-of-the-art human preference learning methods, including Diffusion-DPO, D3PO, and DDPO, by following their original configurations. Since Diffusion-DPO is the only method that reports results based on SDXL, we summarize the comparison results in two tables including Table 1 and Table 2, depending on the choice of the basic diffusion model: either SDXL or SD-1.5. We report all comparison results based on the 500 validation prompts, *i.e.*, validation_unique split of Pick-a-Pic Kirstain et al. [2024], adopted in Wallace et al. [2023].

As shown in Table 1, SPO outperforms Diffusion-DPO across all four chosen AI feedback models: PickScore Kirstain et al. [2024] (general human preference), HPSV2 Wu et al. [2023a] (prompt alignment), ImageReward Xu et al. [2024] (general human preference), and Aesthetic Schuhmann [2022] (visual appeal). For example, when using HPSV2 as the preference rating model, our SPO outperforms Diffusion-DPO by +2.49. Similarly, when using PickScore as the preference model, our SPO surpasses Diffusion-DPO by +0.42, which is significant considering that the gain of Diffusion-DPO over SDXL is approximately +0.69. In addition, we conduct a through user study by requesting 10 users to compare all the generated images side-by-side from three aspects, which include *general preference* (which image do you prefer given the prompt?), *visual appeal* (which image is more visually appealing?) and *prompt alignment* (which image better fits the text description?), and report the win-rate percentage results in Figure 5. To control the cost of human evaluation, we randomly sample ~ 100 prompts from PartiPrompts and ~ 200 prompts from HPSV2 benchmark, respectively. According to these comparison results, we can conclude that our SPO significantly outperforms the previous state-of-the-art Diffusion-DPO based on both various AI feedbacks and human feedbacks.

We illustrate the comparison results with DDPO, D3PO, and Diffusion-DPO based on SD-1.5 in Table 2. We conclude that our SPO achieves the best performance across all AI feedback evaluation results. An interesting observation is that DDPO even outperforms both D3PO and Diffusion-DPO when evaluated with the PickScore preference model.

We further compare some sample image generation results in Figure 6. SPO generates more visually appealing images with a vivid array of colors and fine-grained details. As shown in the previous user study results (Figure 5), the visual appeal of our approach is generally favored. In the following section, we conduct all the ablation experiments based on SD-1.5 if not specified.

5.3 Ablation Study and Analysis

Effect of step-wise resampler. We first study the effect of removing step-wise resampling at each denoising step, *i.e.*, generating k different denoising trajectories from Gaussian noise. We report the comparison results in Table 3, and we observe that the step-wise resampling significantly boosts performance across all four metrics under the random selection scheme. In addition, we empirically find that the random selection scheme is critical for the success of step-wise resampling. By comparing the results in the 1-st row and the 4-th row, we anticipate that the key reason for the effectiveness of the random selection strategy is that it not only removes the trajectory-level dependency but also acts as a kind of effective trajectory augmentation, enriching the win-lose pairs at different denoising steps. We hypothesize that the reason for the inferior performance of only selecting x_{t-1}^w or x_{t-1}^l is that it causes the training to be biased towards the intermediate images that are more preferred or more dispreferred, respectively.

Effect of the step-aware preference model. We verify the importance of the step-aware preference model by replacing it with a step-agnostic preference model that simply predicts the preference order of the denoised sample at the $(t-1)$ -th timestep without using the timestep as a condition. In other words, we remove the dependency on the timestep and the corresponding adaptive layer norm design. We also report the performance of directly applying the original pick-score preference model without fine-tuning on the noisy samples. Table 4 summarizes the comparison results, and we can conclude that the step-aware scheme is important for ensuring accurate estimation of the step-wise preference order at the sampled timesteps.

Effect of number of candidates sampled at each denoising step. To sample effective win-lose pairs during the intermediate denoising timesteps, we obtain a set of candidates $\{x_{t-1}^1, x_{t-1}^2, \dots, x_{t-1}^k\}$ at each step, drawing from the conditional distribution $p_\theta(x_{t-1} | x_t, c, t)$. Then we apply the step-aware preference model to determine the most preferred and the most dispreferred instances among the candidate samples, and use them to establish a win-lose preference pair. Table 5 ablates the effect of varying the number of x_{t-1} samples, k , at each step.

According to Table 5, we can achieve the following conclusions: (i) when increasing k , the discrepancy in the sampled pairs is larger, and the obvious contrast between the preferred x_{t-1} and unpreferred x_{t-1} helps the model better learn human preferences. (ii) when k is too large, selecting the most dispreferred x_{t-1} instance among multiple samples to construct the preference pair tends to result in lower quality images than those generated by the base model on average. Consequently, during training, the “pushing away” effect of the dispreferred image in a preference pair is weakened, causing a degradation in performance.

Effect of the number of inner steps within multi-step-aware preference optimization. We also extend our SPO approach to multi-step SPO that supports a flexible number of denoising steps, *i.e.*, inner steps, before sampling the win-lose pairs. The key reason is that we observe merely denoising one step often fails to generate win-lose pairs with sufficient differences for the state-of-the-art diffusion models like SDXL. Therefore, we study the effect of increasing the number of inner steps from 1 to 6 based on SDXL, which means we sample x_{t-1} , x_{t-2} , x_{t-3} , x_{t-4} , x_{t-5} , and x_{t-6} , respectively. Table 6 reports the detailed comparison results, showing that our approach achieves the best performance when applying ~ 4 inner steps.

Effect of κ choice. Table 7 compares the effect of choosing different timestep ranges, κ , when applying the step-aware preference optimization strategy. We empirically find that the model performance first increases and then drops when applying preference learning during timestep ranges with a higher degree of noise. We analyze the step-aware preference model’s performance during different timesteps and suspect the reason is that the step-wise preference model cannot achieve reliable preference prediction for samples with severe noise, such as those in the timestep range larger than 750.

Effect of win-lose pairs choice. Table 8 compares the effect of using different strategies for choosing win-lose pairs from the candidate set $\{x_{t-1}^1, x_{t-1}^2, \dots, x_{t-1}^k\}$. We can see that selecting the best (most preferred) and the worse (most dispreferred) samples to form the win-lose pairs achieves better performance than random selection.

Computational cost. We use $4 \times$ A100 GPUs, which take ~ 12 and ~ 29.5 hours to train SD-1.5 and SDXL, respectively. Further considering the time (~ 8 and ~ 29 hours for SD-1.5 and SDXL, respectively) used for training the step-aware preference model, the entire training GPU-hours of

SPO-SDXL is less than 10% of the training GPU-hours of Diffusion-DPO (SD-1.5: ~ 384 and SDXL: $\sim 4,800$). This is probably due to the use of step-aware aligned preference labels in SPO.

6 Conclusion

In this paper, we study human preference learning for post-training diffusion models. Existing methods propagate the same preference labels obtained from the final image x_0 to the noisy latents during all the intermediate timesteps. We identified that this process essentially mismatches the denoising performance of individual timesteps with the preference labels, compromising fine-tuning effectiveness. We address this problem by proposing a step-aware preference model and a step-wise resampler to align the preference optimization target with the denoising performance at each timestep. We empirically show that the proposed step-aware preference optimization (SPO) yields superior post-training performance compared to existing methods on both SD-1.5 and SDXL, and is more than $20\times$ times more efficient to train due to more reasonable preference labeling.

References

- Kevin Black, Michael Janner, Yilun Du, Ilya Kostrikov, and Sergey Levine. Training diffusion models with reinforcement learning. *arXiv preprint arXiv:2305.13301*, 2023.
- Chaofeng Chen, Annan Wang, Haoning Wu, Liang Liao, Wenxiu Sun, Qiong Yan, and Weisi Lin. Enhancing diffusion models with text-encoder reinforcement learning. *arXiv preprint arXiv:2311.15657*, 2023.
- Kevin Clark, Paul Vicol, Kevin Swersky, and David J Fleet. Directly fine-tuning diffusion models on differentiable rewards. *arXiv preprint arXiv:2309.17400*, 2023.
- Prafulla Dhariwal and Alexander Nichol. Diffusion models beat gans on image synthesis. *Advances in neural information processing systems*, 34:8780–8794, 2021.
- Ying Fan, Olivia Watkins, Yuqing Du, Hao Liu, Moonkyung Ryu, Craig Boutilier, Pieter Abbeel, Mohammad Ghavamzadeh, Kangwook Lee, and Kimin Lee. Reinforcement learning for fine-tuning text-to-image diffusion models. *Advances in Neural Information Processing Systems*, 36, 2024.
- Amir Hertz, Ron Mokady, Jay Tenenbaum, Kfir Aberman, Yael Pritch, and Daniel Cohen-Or. Prompt-to-prompt image editing with cross attention control. *arXiv preprint arXiv:2208.01626*, 2022.
- Jonathan Ho and Tim Salimans. Classifier-free diffusion guidance. *arXiv preprint arXiv:2207.12598*, 2022.
- Edward J Hu, Yelong Shen, Phillip Wallis, Zeyuan Allen-Zhu, Yuanzhi Li, Shean Wang, Lu Wang, and Weizhu Chen. Lora: Low-rank adaptation of large language models. *arXiv preprint arXiv:2106.09685*, 2021.
- Yuval Kirstain, Adam Polyak, Uriel Singer, Shahbuland Matiana, Joe Penna, and Omer Levy. Pick-a-pic: An open dataset of user preferences for text-to-image generation. *Advances in Neural Information Processing Systems*, 36, 2024.
- Kimin Lee, Hao Liu, Moonkyung Ryu, Olivia Watkins, Yuqing Du, Craig Boutilier, Pieter Abbeel, Mohammad Ghavamzadeh, and Shixiang Shane Gu. Aligning text-to-image models using human feedback. *arXiv preprint arXiv:2302.12192*, 2023.
- Zeyu Liu, Weicong Liang, Zhanhao Liang, Chong Luo, Ji Li, Gao Huang, and Yuhui Yuan. Glyph-by5: A customized text encoder for accurate visual text rendering. *arXiv preprint arXiv:2403.09622*, 2024.
- Long Ouyang, Jeffrey Wu, Xu Jiang, Diogo Almeida, Carroll Wainwright, Pamela Mishkin, Chong Zhang, Sandhini Agarwal, Katarina Slama, Alex Ray, et al. Training language models to follow instructions with human feedback. *Advances in Neural Information Processing Systems*, 35: 27730–27744, 2022.

- William Peebles and Saining Xie. Scalable diffusion models with transformers. In *Proceedings of the IEEE/CVF International Conference on Computer Vision*, pages 4195–4205, 2023.
- Dustin Podell, Zion English, Kyle Lacey, Andreas Blattmann, Tim Dockhorn, Jonas Müller, Joe Penna, and Robin Rombach. Sdxl: Improving latent diffusion models for high-resolution image synthesis. *arXiv preprint arXiv:2307.01952*, 2023.
- Mihir Prabhudesai, Anirudh Goyal, Deepak Pathak, and Katerina Fragkiadaki. Aligning text-to-image diffusion models with reward backpropagation. *arXiv preprint arXiv:2310.03739*, 2023.
- Alec Radford, Jong Wook Kim, Chris Hallacy, Aditya Ramesh, Gabriel Goh, Sandhini Agarwal, Girish Sastry, Amanda Askell, Pamela Mishkin, Jack Clark, et al. Learning transferable visual models from natural language supervision. In *International conference on machine learning*, pages 8748–8763. PMLR, 2021.
- Rafael Rafailov, Archit Sharma, Eric Mitchell, Christopher D Manning, Stefano Ermon, and Chelsea Finn. Direct preference optimization: Your language model is secretly a reward model. *Advances in Neural Information Processing Systems*, 36, 2024.
- Robin Rombach, Andreas Blattmann, Dominik Lorenz, Patrick Esser, and Björn Ommer. High-resolution image synthesis with latent diffusion models. In *Proceedings of the IEEE/CVF conference on computer vision and pattern recognition*, pages 10684–10695, 2022.
- Christoph Schuhmann. Laion-aesthetics. <https://laion.ai/blog/laion-aesthetics/>, 2022. Accessed: 2023 - 11- 10.
- John Schulman, Filip Wolski, Prafulla Dhariwal, Alec Radford, and Oleg Klimov. Proximal policy optimization algorithms. *arXiv preprint arXiv:1707.06347*, 2017.
- Jiaming Song, Chenlin Meng, and Stefano Ermon. Denoising diffusion implicit models. *arXiv preprint arXiv:2010.02502*, 2020.
- Bram Wallace, Meihua Dang, Rafael Rafailov, Linqi Zhou, Aaron Lou, Senthil Purushwalkam, Stefano Ermon, Caiming Xiong, Shafiq Joty, and Nikhil Naik. Diffusion model alignment using direct preference optimization. *arXiv preprint arXiv:2311.12908*, 2023.
- Xiaoshi Wu, Yiming Hao, Keqiang Sun, Yixiong Chen, Feng Zhu, Rui Zhao, and Hongsheng Li. Human preference score v2: A solid benchmark for evaluating human preferences of text-to-image synthesis. *arXiv preprint arXiv:2306.09341*, 2023a.
- Xiaoshi Wu, Keqiang Sun, Feng Zhu, Rui Zhao, and Hongsheng Li. Better aligning text-to-image models with human preference. *arXiv preprint arXiv:2303.14420*, 2023b.
- Jiazheng Xu, Xiao Liu, Yuchen Wu, Yuxuan Tong, Qinkai Li, Ming Ding, Jie Tang, and Yuxiao Dong. Imagereward: Learning and evaluating human preferences for text-to-image generation. *Advances in Neural Information Processing Systems*, 36, 2024.
- Kai Yang, Jian Tao, Jiafei Lyu, Chunjiang Ge, Jiaxin Chen, Qimai Li, Weihan Shen, Xiaolong Zhu, and Xiu Li. Using human feedback to fine-tune diffusion models without any reward model. *arXiv preprint arXiv:2311.13231*, 2023.
- Shentao Yang, Tianqi Chen, and Mingyuan Zhou. A dense reward view on aligning text-to-image diffusion with preference. *arXiv preprint arXiv:2402.08265*, 2024.
- Jiahui Yu, Yuanzhong Xu, Jing Yu Koh, Thang Luong, Gunjan Baid, Zirui Wang, Vijay Vasudevan, Alexander Ku, Yinfei Yang, Burcu Karagol Ayan, et al. Scaling autoregressive models for content-rich text-to-image generation. *arXiv preprint arXiv:2206.10789*, 2(3):5, 2022.

7 Supplementary

7.1 Illustrating the Detailed Prompts

We summarize the detailed text prompts used in Figure 1 in the following Table 9.

Image	Prompt
Fig 1, Row 1, Col1	paw patrol. "This is some serious gourmet". 2 dogs holding mugs.
Fig 1, Row 1, Col2	little tiny cub beautiful light color White fox soft fur kawaii chibi Walt Disney style, beautiful smiley face and beautiful eyes sweet and smiling features, snuggled in its soft and soft pastel pink cover, magical light background, style Thomas kinkade Nadja Baxter Anne Stokes Nancy Noel realistic
Fig 1, Row 1, Col3	Full Portrait of Consort Chunhui by Giuseppe Castiglione, symmetrical face, ancient Chinese painting, single face, insanely detailed and intricate, beautiful, elegant, artstation, character concept in the style illustration by Miho Hirano, Giuseppe Castiglione –ar 9:16
Fig 1, Row 1, Col4	Surfer robot dude in the crest of a wave, cinematic, sunny, –ar 16:9
Fig 1, Row 1, Col5	a photo of a frog holding an apple while smiling in the forest
Fig 1, Row 2, Col1	185764, ink art, Calligraphy, bamboo plant :: orange, teal, white, black –ar 2:3 –uplight
Fig 1, Row 2, Col2	large battle Mecha helping with the construction of the Colossus of Rhodos standing above the entry of a harbor, hundreds of ancient workers on scaffolding surrounding the colossus, ancient culture, sunny weather, matte painting, highly detailed, cgsociety, hyperrealistic, –no dof, –ar 16:9
Fig 1, Row 2, Col3	A 3D Rendering of a cockatoo wearing sunglasses. The sunglasses have a deep black frame with bright pink lenses. Fashion photography, volumetric lighting, CG rendering.
Fig 1, Row 2, Col4	a golden retriever dressed like a General in the north army of the American Civil war. Portrait style, looking proud detailed 8k realistic super realistic Ultra HD cinematography photorealistic epic composition Unreal Engine Cinematic Color Grading portrait Photography UltraWide Angle Depth of Field hyperdetailed beautifully colorcoded insane details intricate details beautifully color graded Unreal Engine Editorial Photography Photography Photoshoot DOF Tilt Blur White Balance 32k SuperResolution Megapixel ProPhoto RGB VR Halfrear Lighting Backlight Natural Lighting Incandescent Optical Fiber Moody Lighting Cinematic Lighting Studio Lighting Soft Lighting Volumetric ContreJour Beautiful Lighting Accent Lighting Global Illumination Screen Space Global Illumination Ray Tracing Optics Scattering Glowing Shadows Rough Shimmering Ray Tracing Reflections Lumen Reflections Screen Space Reflections Diffraction Grading Chromatic Aberration GB Displacement Scan Lines Ray Traced Ray Tracing Ambient Occlusion AntiAliasing FKA TXAA RTX SSAO Shaders
Fig 1, Row 2, Col5	A rock formation in the shape of a horse, insanely detailed,
Fig 1, Row 3, Col1	a gopro snapshot of an anthropomorphic cat dressed as a firefighter putting out a building fire
Fig 1, Row 3, Col2	a desert in a snowglobe, 4k, octane render :: cinematic –ar 2048:858
Fig 1, Row 3, Col3	cat, cute, child, hat
Fig 1, Row 3, Col4	watercolour beaver with tale, white background
Fig 1, Row 3, Col5	corporate office ralph goings – aspect 3:2
Fig 1, Row 4, Col1	there once was a fly on the wall, I wonder, why didn't it fall, Because its feet stuck, Or was it just luck, Or does gravity miss things so small, high realistic, high detailed, high contrast, unreal render –ar 16:9
Fig 1, Row 4, Col2	lush landscape with mountains with cherry trees by Miyazaki Nausicaa Ghibli, 王ランキング, ranking of kings, spirited away, breath of the wild style, epic composition, clean –w 1024 –h 1792 –no people
Fig 1, Row 4, Col3	what i dream when i close my eyes to sleep
Fig 1, Row 4, Col4	cute cat jumped off plane in parachute, exaggerated expression, photo realism, side angle, epic drama
Fig 1, Row 4, Col5	Full body, a Super cute little girl, wearing cute little giraffe pajamas, Smile and look ahead, ultra detailed sky blue eyes, 8k bright front lighting, fine luster, ultra detail, hyper detailed 3D rendering s750,

Table 9: Detailed prompts used for generated images in Figure 1.

7.2 Application to Design Image Generation

We verify the generalization of our approach by simply replacing the original SDXL within the very recent Glyph-SDXL Liu et al. [2024] with our SPO-SDXL. We observe the visual appealing of the entire graphic design image consistently improves and we show some representative examples in Figure 7. We also plan to combine our SPO-SDXL with various challenging visual generation tasks based on SDXL in the future.



Figure 7: Qualitative comparison between Glyph-SDXL and Glyph-SDXL + SPO in graphic design image generation tasks. We can see that the background image quality is significantly improved with our approach.